Tellus SERIES A DYNAMIC METEOROLOGY AND OCEANOGRAPHY
PUBLISHED BY THE INTERNATIONAL METEOROLOGICAL INSTITUTE IN STOCKHOLM

Tellus (2011), 63A, 921–938
Printed in Singapore. All rights reserved

TELLUS

Climatological aspects of cyclogenesis near Adélie Land Antarctica

By DAVID H. BROMWICH[1,2]*, DANIEL F. STEINHOFF[1,2], IAN SIMMONDS[3], KEVIN KEAY[3] and RYAN L. FOGT[4], [1]*Polar Meteorology Group, Byrd Polar Research Center, The Ohio State University, Columbus, Ohio, USA;* [2]*Atmospheric Sciences Program, Department of Geography, The Ohio State University, Columbus, Ohio, USA;* [3]*School of Earth Sciences, University of Melbourne, Melbourne, Victoria, Australia;* [4]*Department of Geography, Ohio University, Athens, Ohio, USA*

(Manuscript received 22 December 2010; in final form 8 July 2011)

ABSTRACT

The Adélie Land coastal region of Antarctica is one of the most prominent cyclogenesis regions in the Southern Hemisphere, and is adjacent to the continent's most intense katabatic wind regime. However, the physical mechanisms responsible for cyclogenesis are not known. A manual analysis of cyclogenesis for the 2003–2005 period using output from the Antarctic Mesoscale Prediction System (AMPS) identifies two primary patterns of cyclogenesis near the Adélie Land coast. For "secondary development" cyclones, enhanced low-level cyclonic vorticity and baroclinicity result from the combination of an existing synoptic-scale cyclone to the west, coastal barrier winds and katabatic winds. "Lee cyclogenesis" occurs near 152°E on the cyclonic-shear side of the Adélie Land katabatic jet, where a low-level warm potential temperature anomaly sets up a lee trough that becomes mobile with the arrival of upper-level synoptic-scale forcing. The representation of both "secondary development" and "lee cyclogenesis" cyclones in an automated cyclone-tracking scheme is explored, where it is found that the automated scheme overestimates cyclogenesis for this region. The location of the Antarctic coastal cyclogenesis maximum near Adélie Land is due to the unique juxtaposition of the extraordinary katabatic wind regime and dissipating synoptic-scale cyclones to the west.

1. Introduction

While early observational studies of Southern Hemisphere cyclone activity found a general pattern of cyclogenesis in mid-latitudes and cyclolysis in coastal Antarctica (Taljaard, 1967; Streten, 1968; Streten and Troup, 1973), later studies utilizing higher spatial and temporal resolution satellite imagery found (primarily mesoscale) cyclogenesis near the Antarctic coast (Carleton, 1979; Carleton and Carpenter, 1990; Carleton and Fitch, 1993; Carleton and Song, 1997). Further details came from automated cyclone tracking schemes, which use numerical methods to determine the location of cyclones through identification of minimum pressure on MSLP surfaces or maximum cyclonic vorticity on lower-tropospheric isobaric surfaces in gridded atmospheric products (e.g. Le Marshall and Kelly, 1981; Lambert, 1988; Le Treut and Kalnay, 1990; Jones and Simmonds, 1993; Sinclair, 1994, 1995, 1997).

Cyclone tracking schemes have identified an intense synoptic-scale cyclogenesis maximum near the Antarctic coast at 150°E. Simmonds et al. (2003), using a refined version of the Melbourne University (MU) tracking scheme (Murray and Simmonds, 1991) and NCEP-2 reanalysis data from 1979 to 2000, find a cyclogenesis maximum between 60°S–65°S and 140°E–150°E, most prevalent in winter. This region is one of the few areas south of 60°S that experiences net cyclogenesis (more cyclogenesis than cyclolysis) annually. Hoskins and Hodges (2005) use the ERA-40 reanalysis and the tracking scheme of Hodges (1995, 1996, 1999), and find a maximum in cyclone track density in both 850 hPa relative vorticity and MSLP between 140°E and 180° along the immediate Antarctic coast in all seasons except summer. The largest cyclogenesis and cyclolysis density regions around Antarctica at both 850 hPa and 500 hPa are found near 150°E and 115°E, respectively. Wernli and Schwierz (2006) use 1958–2001 ERA-40 data and a tracking scheme based on the outermost closed contour of MSLP, and find similar Antarctic cyclone density, cyclogenesis and cyclolysis patterns as Simmonds et al. (2003) and Hoskins and Hodges (2005). Uotila et al., (2009, 2011) present tracking metrics from the MU tracking scheme using output from the Antarctic Mesoscale Prediction System (AMPS, Powers et al., 2003). A net cyclogenesis region is once again located over the marginal sea ice zone between 140°E and 150°E, with an Antarctic coastal maximum in cyclone track

*Corresponding author.
e-mail: bromwich@polarmet1.mps.ohio-state.edu
DOI: 10.1111/j.1600-0870.2011.00537.x

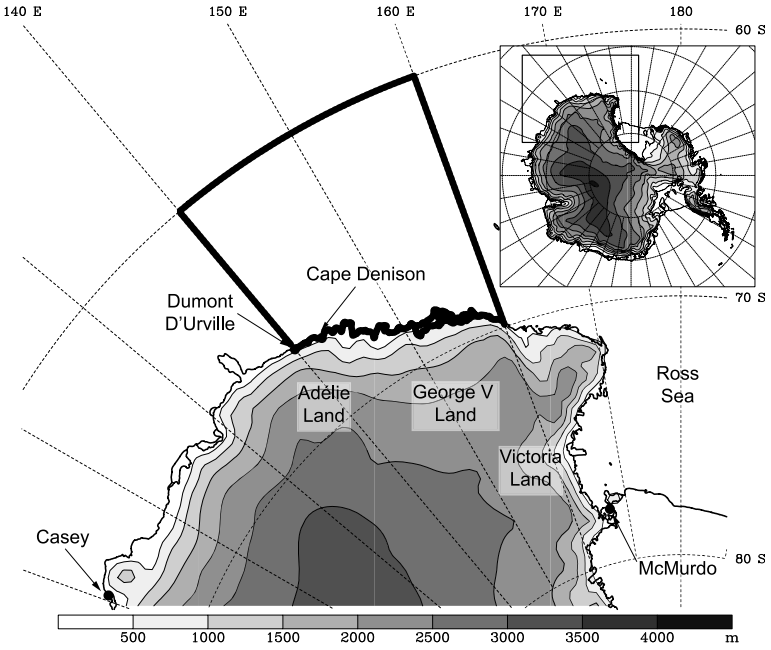

Fig. 1. Map of Adélie Land region of Antarctica. Inset map shows region in relation to rest of Antarctic continent. Terrain height (shaded) in metres. Bold outline represents manual cyclone tracking study area (140°E–160°E, 60°S-coast).

density for both synoptic-scale and mesoscale cyclones as well. Yuan et al. (2009), using a tracking scheme with surface pressure fields blended between those derived from QuikSCAT winds (UWQS, Patoux et al., 2003, 2009) and ECMWF operational model fields, find a cyclogenesis maximum near Adélie Land in all seasons. Irving et al. (2010) assess mesoscale cyclone activity using UWQS pressure fields with the MU tracking scheme. They find a regional maximum in mesoscale system density in all seasons between 110°E and 140°E.

Little discussion has taken place regarding the physical mechanisms responsible for the prominent cyclogenesis near the coast at 150°E (see Fig. 1 for geographical orientation). Hoskins and Hodges (2005) suggest that this cyclogenesis region results from the propagation of cyclones towards the Antarctic coast upstream of Adélie Land and the enhancement over depth of the baroclinicity there, and that katabatic winds have little influence on cyclogenesis. The Adélie Land katabatic wind regime is one of the most intense and persistent sea-level wind regimes in the world, as first documented by Sir Douglas Mawson's Australasian expedition of 1912–1913 at Cape Denison (67.01°S, 142.67°E) in 'The Home of the Blizzard' (Mawson, 1915) and by Madigan (1929). The annual average wind speed of almost 20 m s^{-1} and high directional constancy have been confirmed by automatic weather station observations (Keller et al., 1997) and by Parish and Walker (2006). This extraordinary katabatic wind regime represents a 'confluence zone', resulting from an enhanced supply of negatively buoyant air upstream of the coastal region. The link between offshore katabatic winds and mesoscale cyclogenesis in Antarctica has been explored extensively, primarily near Terra Nova Bay, over the Ross Ice Shelf, near the Antarctic Peninsula, and over the Weddell Sea (see Carrasco et al., 2003 for a detailed review of Antarctic mesoscale cyclones). Several physical mechanisms have been proposed, including generation of a low-level baroclinic zone (Bromwich, 1989, 1991; Carrasco and Bromwich, 1993; Fantini and Buzzi, 1993; Gallée, 1995, 1996; Turner et al., 1993, 1998; Carrasco et al., 1997a,b), formation on the cyclonic-shear side of the katabatic jet (Carrasco, 1994; Heinemann and Klein, 2003) and vortex stretching (Carrasco and Bromwich, 1995; Engels and Heinemann, 1996; Klein and Heinemann, 2001).

The relationship between katabatic winds and synoptic-scale cyclones is less clear. Carleton (1992) and Parish and Bromwich (1998, 2007) suggest a link between the low-level flow off of the continent and cyclogenesis through development of the offshore easterly wind regime and enhancement of baroclinicity (Murphy and Simmonds, 1993). Time-averaged and zonally averaged low-level convergence and upward vertical motion occurs just north of the continent, concentrated in the lowest 1 km, as a result of the convergence of drainage flow. A series of GCM experiments by Walsh et al. (2000) find reduced baroclinicity and cyclone activity around Antarctica when Antarctic topography is lowered or removed. Parish and Walker (2006) specifically mention the interaction between the low-level circulation and cyclogenesis for the Adélie Land coastal region in conjunction with two examples of cyclogenesis.

In this study, physical mechanisms responsible for cyclogenesis near Adélie Land are explored through the use of composite analysis with AMPS output. Emphasis is placed on the impact of the low-level coastal wind regime (which includes the Adélie Land katabatic wind regime) on cyclone development. It will be shown that the combination of the ambient synoptic-scale flow, the blocking effect of the Antarctic continent, and the Adélie

Land katabatic wind regime are integral for cyclogenesis in this region. Thus, both existing and new concepts for Antarctic cyclogenesis are provided. In addition, comparisons are done between cyclones identified from manual identification and those from an automated cyclone finding and tracking scheme, and insights are presented into how the automated scheme is representing cyclone development in the region.

2. Data and methods

2.1. AMPS/Polar MM5

AMPS is a joint effort between the Mesoscale and Microscale Meteorology (MMM) Division of the National Center for Atmospheric Research (NCAR) and the Polar Meteorology Group of the Byrd Polar Research Center at The Ohio State University. During the study period, AMPS employs Polar MM5, a version of the fifth-generation Pennsylvania State University-NCAR Mesoscale Model (Grell et al., 1995) optimised for use in polar regions by the Polar Meteorology Group (Bromwich et al., 2001; Cassano et al., 2001). AMPS provides forecast guidance for United States Antarctic Program (USAP) flight operations. In recent years, use of AMPS has grown beyond just U.S. operations to include use by the international Antarctic forecasting community. AMPS has also been used in Antarctic scientific research applications (e.g. Bromwich et al., 2003; Monaghan et al., 2005; Steinhoff et al., 2008; Fogt and Bromwich, 2008; Schlosser et al., 2008). Polar MM5 includes several modifications for use in polar regions. These changes include a modified parameterization for the prediction of ice cloud fraction, improved cloud-radiation interactions, an optimal stable boundary layer treatment, improved calculation of heat transfer through snow and ice surfaces, and the allowance for fractional sea ice coverage, known to be an important determinant for the mean distribution of surface pressure (e.g. Simmonds and Budd, 1991). Guo et al. (2003) evaluate Polar MM5 performance over Antarctica for a 1-year period (1993) on a 60-km resolution domain and show that the intraseasonal and interseasonal variability in pressure, temperature, wind and moisture are well-simulated.

The AMPS Polar MM5 domain with 220 $\times$ 208 gridpoints in the horizontal and at 30-km resolution is used here. There are 32 full sigma levels in the vertical, with 11 levels in the lowest 1000 m. The lowest half-sigma level is about 13 m above the surface. As a result of work done by the Polar Meteorology Group at Ohio State, the upper boundary condition was changed in May 2003 from a rigid lid at 100 hPa to a nudging upper boundary condition at 50 hPa that is adjusted using GFS forecast temperatures in the highest 8 sigma levels (with two model levels added in the process). This was done to prevent reflection of upward propagating gravity waves. AMPS Polar MM5 is initialized twice daily at 0000 and 1200 UTC. The initial and boundary conditions are derived from the NCEP Global Forecasting System (GFS) model. Prior to the 1200 UTC 27 May 2004 initialization, the GFS first-guess field is objectively reanalysed with the available observations using a multiquadric technique (Nuss and Titley, 1994). From 1200 UTC 27 May 2004 forward, 3-D Variational Data Assimilation (3DVAR, Barker et al., 2004) is used for AMPS initialization. The observations available for assimilation into AMPS include reports from radiosondes, surface SYNOP reports, AWS observations, ship reports and buoys. Satellite-derived cloud-track winds are also assimilated into the largest domain. AMPS ingests sea ice data daily from the National Snow and Ice Data Center for its fractional sea ice depiction. Bromwich et al. (2005) perform a statistical evaluation of 2 years of AMPS Polar MM5 forecasts on the 30-km domain over the Antarctic continent, and show that the basic meteorological variables correlate well with surface and upper-air radiosonde observations. Systematic validation has not been undertaken over the Southern Ocean, where reanalyses and global climate models underestimate cloud and albedo over the Southern Hemisphere extratropics (Trenberth and Fasullo, 2010). Too much solar radiation reaching the ocean in high latitudes, combined with too little in lower latitudes, results in an underestimation of baroclinic activity over the Southern Ocean. Such deficiencies may extend to AMPS from the GFS.

2.2. Manual cyclone identification

In order to categorize cyclogenesis in the Adélie Land region, AMPS output is used in the manual identification of cyclones for the construction of composite cyclones. Plots of the AMPS surface pressure field for the 3-year period 2003–2005 are analysed for cyclogenesis. All available model runs initialized at 0000 UTC daily are used, with output every 6 h. The 12, 18, 24 and 30 h forecasts from each model run are used preferentially; if these are not available then later forecasts are used up to 72 h. Of 4384 potential forecasts during the 3-year period, 4244 are available (about 97%). Minima in the surface pressure field forming in the region 60°S to the coast and between 140°E and 160°E are recorded if there are two closed isobars (2 hPa contour interval) and if two closed isobars persist for at least 12 h. For cyclones along the immediate coast, where a closed circulation may not exist, a centre must be identified with five surrounding pressure contours. Direct comparisons of the manually identified cyclones and cyclones identified with the MU tracking scheme (using AMPS) is done in Section 4 to give some perspective on the characteristics and validity of the manually identified cyclones, while also identifying issues with automated tracking methods near coastal Antarctica.

2.3. JRA-25 and Melbourne University cyclone finding and tracking scheme

The Japanese 25-year re-analysis (JRA-25, Onogi et al., 2007) is a joint project between the Japan Meteorological Agency (JMA)

and the Central Research Institute of Electric Power Industry (CRIEPI). JRA-25 is at T106 spectral truncation (about 125 km resolution) with 40 vertical levels. Variables such as MSLP are available at 1.25° and 2.5° resolution. In this study, the MU tracking scheme was applied to 2.5° MSLP data from 1979 to 2007, followed by bilinear interpolation of the cyclone variables to 0.5° by 0.5°, for comparison with AMPS. JRA-25 is found to compare favourably with other reanalysis data sets in the Southern Hemisphere (Bromwich et al., 2007).

The Melbourne University Cyclone Finding and Tracking Scheme is an objective and automated scheme that finds and tracks cyclones, defined as minima of MSLP, from operational or reanalysis data sets. Description of the scheme can be found in Murray and Simmonds (1991), with refinements described in Simmonds et al. (1999) and Simmonds and Murray (1999). Gridpoint local maxima of the Laplacian of the pressure field are found, which represent relative minima in the pressure field. The cyclone centre for 'closed' lows is defined as the minimum pressure, whereas for 'open' cyclones it is the inflection point of the pressure field. Cyclones must last at least 24 h, and cyclones in regions of terrain height of 1 km or greater are discarded, since the reduction of pressure to sea level is inaccurate over the inland plateau of Antarctica. In addition, cyclones over regions of sloping terrain have a more restrictive concavity criterion applied. Theoretically, the smallest cyclone radius that the tracking scheme can identify is the grid spacing (90 km). However, the tracking scheme smoothes input fields, and Uotila et al. (2011) found a minimum radius of about 1.2° latitude (about 133 km). Cyclones are tracked between 6 hourly analyses, and statistics including system density (mean number of cyclones found in a unit area per analysis), cyclogenesis and cyclolysis are found after the tracking is completed. Instruction parameters for the tracking scheme are listed in Uotila et al. (2009, table 1). Because different domains are used in the manual (60 km) and automated (90 km) tracking, direct comparison between the manual and automated tracking schemes will suffer from these differences.

3. Composite analysis

A total of 132 cyclones are identified from manual examination of AMPS surface pressure charts, and these cyclones have been categorized into five distinct development patterns. These categories feature baroclinic development well away from the Antarctic coast, either from systems moving in from the north or from the west. These cases will not be discussed further. The two most frequent categories feature development near the Antarctic coast, and these two categories will be explored below through composite analysis. Both sets of composites are representative of the respective pattern of development found in all cases, and not dominated by any particular strong events, although the location and intensity of the features vary between cases.

3.1. Secondary development

53 cyclones are identified in the study area (140°E–160°E, 60°S-coast) as 'secondary development', analogous to cyclone development along the warm front of an occluded cyclone (e.g. Carlson, 1991, p. 206). Any instance of a dissipating cyclone west of the study area and near the coast (so that a low-level barrier jet is apparent) with cyclogenesis in the study area is categorized as secondary development. Sea-level pressure, potential temperature, and wind vector composites from the lowest model level ($\sigma = 0.9983$, about 13 m AGL) from −12 h (12 h before genesis) to +12 h at 6-h intervals are shown in Fig. 2. Twelve hours prior to genesis (Fig. 2a), an existing cyclone is located offshore near 120°E. To the east of the existing cyclone, between 125°E and 145°E, there is an easterly jet of 15–20 m s^{-1} adjacent to the coast. The easterly jet is a barrier wind (Schwerdtfeger, 1984). Cold air is entrained from the east and from the katabatic outflow into the barrier jet. To the north, warm air advection is occurring, associated with a northerly flow component in the northeastern sector of the cyclone. Six hours later (Fig. 2b), the existing cyclone remains nearly stationary near 120°E and weakens. This sequence of events continues to genesis time (Fig. 2c), where the new cyclone is breaking away to the east, centred near 145°E. Over the next 12 h (Fig. 2d and e), the new cyclone moves over the sea ice ESE towards the Ross Sea.

Figure 2a–c suggest that cyclonic shear vorticity and the meridional temperature gradient both increase at low levels east of the existing cyclone, favouring cyclogenesis there. Figure 3a–c show cyclonic relative vorticity from $\sigma = 0.9791$, about 155 m AGL, for −12, −6 and 0 h. Cyclonic relative vorticity is largest in the region north of the barrier wind, between 130°E and 140°E, shifting eastward with time. Vorticity is largest at −6 h, then decreases by 0 h and beyond. To discern the physical processes responsible for the region of large cyclonic vorticity, terms from the vorticity equation (e.g. Holton 1992, p. 103) have been calculated for all cases. The vorticity equation in height coordinates is

$$\begin{aligned}\underset{\text{NET}}{\frac{\partial \zeta}{\partial t}} = &\underset{\text{ADV}}{-\mathrm{V}\cdot\nabla(\zeta+f)} \underset{\text{VER}}{-w\frac{\partial \zeta}{\partial z}} \underset{\text{DIV}}{-(\zeta+f)(\nabla\cdot\mathrm{V})} \\ &\underset{\text{TILT}}{-\left(\frac{\partial w}{\partial x}\frac{\partial v}{\partial z}-\frac{\partial w}{\partial y}\frac{\partial u}{\partial z}\right)} \\ &\underset{\text{SOL}}{+\frac{1}{\rho^2}\left(\frac{\partial \rho}{\partial x}\frac{\partial p}{\partial y}-\frac{\partial \rho}{\partial y}\frac{\partial p}{\partial x}\right)} \underset{\text{COR}}{-v\frac{\partial f}{\partial y}} + \underset{\text{FRC}}{\mathrm{F}_\zeta} \end{aligned} \quad (1)$$

where 'ADV' is the horizontal advection term, 'VER' is vertical advection, 'DIV' is the divergence term, 'TILT' is the tilting term, 'SOL' is the solenoidal term, 'COR' is related to the meridional variation of the Coriolis parameter and 'FRC' represents frictional dissipation. The sum of these terms results in the vorticity tendency ('NET'). The terms are calculated for the region

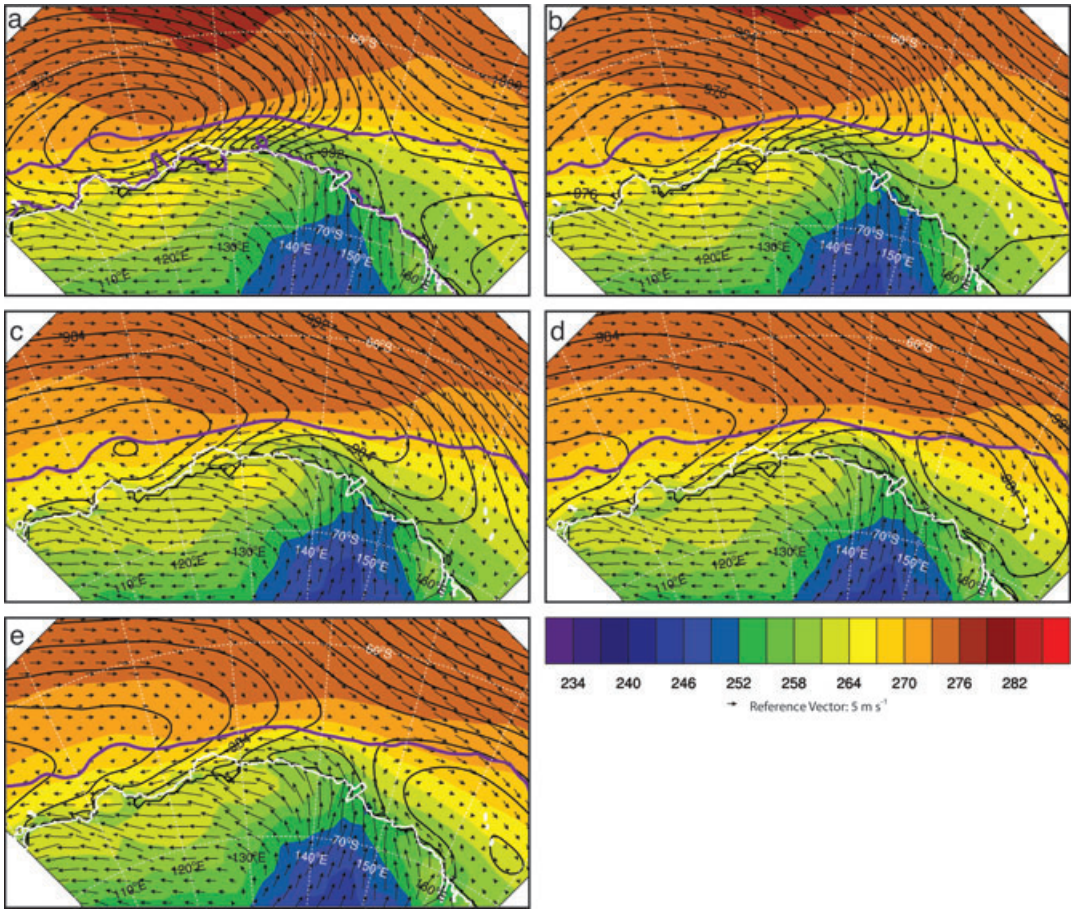

Fig. 2. 'Secondary Development' composites of sea-level pressure (hPa, black contours, contour interval 2 hPa), potential temperature (K, colour shaded) at $\sigma = 0.9983$ (about 13 m AGL) and wind vectors (black arrows) at $\sigma = 0.9983$ at (a) −12 h, (b) −6 h, (c) 0 h, (d) +6 h and (e) +12 h. Composite 50% sea ice concentration isopleth delineated by purple line. Note that map projection is rotated 45° clockwise from Fig. 1 for clarity.

bounded by 130°E–140°E and 63°S–66°S for all cases, and then composited. The results for −12, −6 and 0 h are shown in Fig. 4. (Note that in the Southern Hemisphere, cyclonic vorticity is associated with negative vorticity values). The divergence term contributes most to cyclonic vorticity generation throughout the time period, with small contributions at −12 and −6 h from the tilting term. Anticyclonic vorticity is generated by the advection term, vertical transport and friction. The solenoidal and Coriolis terms have negligible effect, and are not shown. The net result is a generation rate of cyclonic vorticity of about -4×10^{-9} s^{-2} at −12 h, about -1×10^{-9} s^{-2} at −6 h and $+1 \times 10^{-9}$ s^{-2} at 0 h. These results imply maximum cyclonic vorticity just after −6 h, which agrees with Fig. 3.

The physical interpretation of Fig. 4 is clear from Fig. 2. Mass convergence is associated with poleward flow east of the existing cyclone being blocked by the Antarctic continent, and from the Adélie Land katabatic wind, which is directed offshore and then deflected to the left by the Coriolis effect and the pressure gradient force. The advection term is the largest anticyclonic contribution, resulting from the advection of weaker cyclonic vorticity into the area from the north (Fig. 3). The general contribution of each term agrees with a similar analysis for an Antarctic mesoscale cyclogenesis event by Heinemann and Klein (2003).

Previous studies have shown that the Antarctic coastal region near 150°E features the largest lower-tropospheric baroclinicity of the entire Southern Hemisphere extratropics in winter (Berbery and Vera, 1996; Nakamura and Shimpo, 2004; Lim and Simmonds, 2007; Kidston et al., 2009; Simmonds and Lim, 2009). Here, we investigate the effect of baroclinicity upon secondary development. We use the Eady growth rate as a measure of baroclinicity (Eady, 1949),

$$\sigma_{\mathrm{Eady}} = 0.31 \frac{M^2}{N}, \tag{2}$$

where N is the Brunt-Väisälä frequency and M^2 is a measure of the meridional potential temperature gradient $(-g\,\mathrm{d}\theta/\theta\,\mathrm{d}y)$, which from application of the thermal wind equation replaces the zonal wind shear typically used in the definition. This is

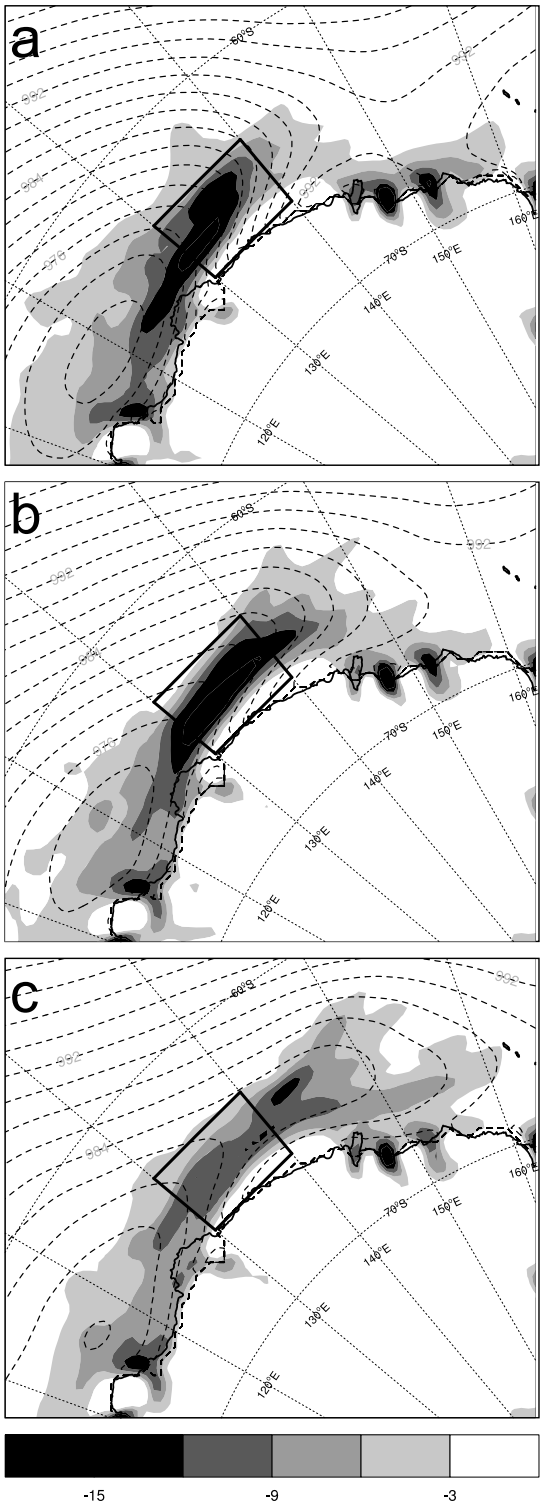

Fig. 3. 'Secondary Development' composites of relative vorticity (10^{-5} s^{-1}, negative values only, shaded) at $\sigma = 0.9791$ (about 155 m AGL) and sea-level pressure (hPa, dashed contours, contour interval 2 hPa) at (a) −12 h, (b) −6 h and (c) 0 h. Box represents averaging region for vorticity tendency equations calculations in Fig. 4.

done, as in Lim and Simmonds (2007) and Simmonds and Lim (2009), because of mechanical wind shear in coastal regions that is not in thermal wind balance. Figure 5 shows composites of the Eady growth rate at −12 h, −6 h and 0 h at 900 hPa. The Eady growth rate is calculated for all individual cases and then composited, avoiding biases from use of the time-mean flow (Simmonds and Lim, 2009). At all three times, Eady growth rate is maximized offshore between 130°E and 140°E. At −6 and 0 h a wedge of lower values extends from the southeast, associated with the strong stability of the katabatic wind regime.

While the Antarctic coastal zone generally consists of strong low-level baroclinicity, this baroclinicity is enhanced during secondary development with a strong meridional temperature gradient and weak stability in the warm sector. The meridional temperature gradient is strengthened from warm air advection from the north in the eastern sector of the cyclone, as well as cold air advection from the Adélie Land katabatic wind regime (Fig. 2a–c). Eady growth rate values in Fig. 5, calculated from cyclogenesis cases occurring year-round, are comparable with those found for winter by Lim and Simmonds (2007) and Simmonds and Lim (2009). Therefore, secondary development is largely responsible for the enhanced baroclinicity of the Adélie Land coastal region. Note from Fig. 2 that cyclogenesis occurs in the marginal sea ice zone, denoted by the purple line. Low-level baroclinicity is enhanced in the marginal sea ice zone, through oppositely directed vertical fluxes of sensible and latent heat on each side of the cyclone (Yuan et al., 2009). Previous research has identified a positive relationship between sea ice and cyclogenesis, mainly through sensitivity studies (Carleton, 1983, 1992; Simmonds and Wu, 1993; Watkins and Simmonds, 1995; Menendez et al., 1999; Hudson and Hewitson, 2001). However, the forcing of the sea ice distribution by atmospheric stresses (katabatic winds and meridional flow associated with cyclones) dominates the effect of sea ice upon cyclone activity (Godfred-Spenning and Simmonds, 1996; Kidston et al., 2009), especially on larger spatial scales (Uotila et al., 2011). It is inferred that the sea ice is a weak positive feedback on cyclone activity.

To diagnose the forcing for large-scale vertical motion associated with the composite cyclone, an analysis of Q-vector convergence is performed. Forcing for vertical motion in the quasi-geostrophic (QG) omega equation can be expressed as twice the convergence of the Q-vector, with the Q-vector defined as

$$\mathbf{Q} = -\frac{R}{P}\left[\left(\frac{\partial \mathbf{V}_g}{\partial x}\cdot\nabla T\right)\mathbf{i} + \left(\frac{\partial \mathbf{V}_g}{\partial y}\cdot\nabla T\right)\mathbf{j}\right] \quad (3)$$

where R is the gas constant, p is pressure, $\boldsymbol{V}_g$ is the geostrophic wind vector and T is temperature. Q-vector convergence contains the total forcing for vertical motion in the QG system (Hoskins et al., 1978). Figure 6a–c show Q-vector convergence for the 400–600 hPa layer for composite hours −12, 0 and +12. At −12 h, a well-defined region of Q-vector convergence exists east of the cyclone centre (130°E to 145°E), implying upward

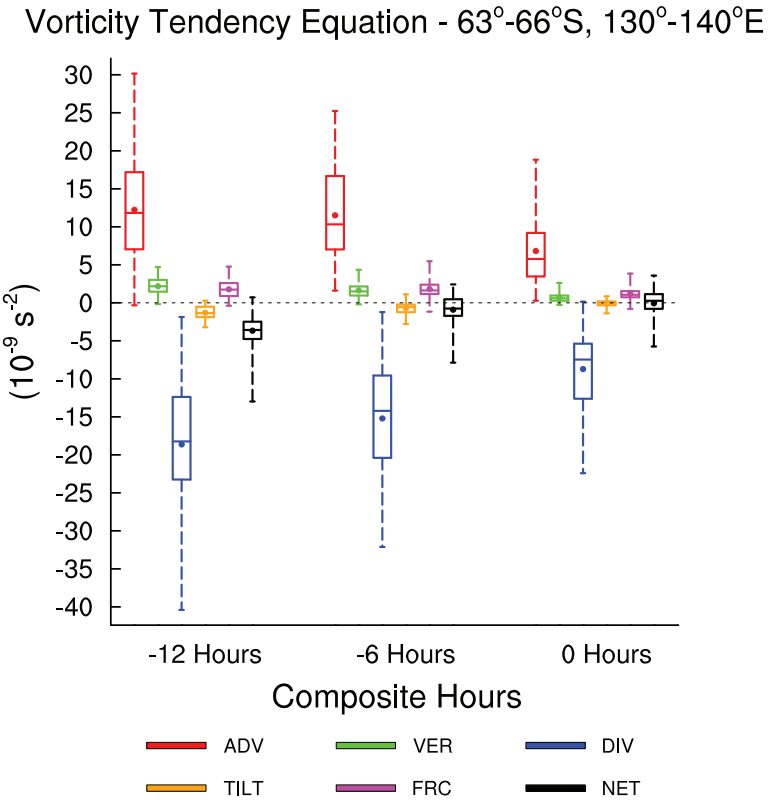

Fig. 4. Box-and-whisker plot of terms from the vorticity tendency equation for 'secondary development' cyclogenesis cases at hours −12, −6 and 0. Individual terms are described in the text. Boxes represent the upper and lower quartiles, horizontal lines inside boxes represent the median, and extension of dashed lines represent the minimum and maximum values. Dots represent the mean value for all cases. Note that negative values represent cyclonic vorticity in the Southern Hemisphere.

vertical motion (Fig. 6a). By 0 h (Fig. 6b), there is a dipole of Q-vector convergence/divergence over the developing cyclone, with Q-vector convergence over the centre near 145°E and farther east, and Q-vector divergence upstream (west) of the developing cyclone. The positioning of this dipole implies deepening of the cyclone, as quasi-geostropic forcing for upward vertical motion is maximized in the vicinity of the cyclone centre. The cyclone signature in the SLP field and the Q-vector convergence pattern are both weakly defined at +12 h (Fig. 6c), as the cyclone tracks begin to diverge, however there is still evidence of Q-vector convergence near the SLP minimum.

In summary, 'secondary development' cyclogenesis results from a combination of favourable conditions: enhanced low-level cyclonic vorticity and baroclinicity, and quasi-geostrophic forcing aloft. While the close proximity of the existing cyclone to the Antarctic coast provides for much of the increase in cyclonic vorticity and baroclinicity, the role of the Adélie Land katabatic wind regime cannot be discounted. It contributes to convergent flow that is the primary forcing for cyclonic vorticity generation, along with increasing baroclinicity by entraining cold air into the coastal barrier jet.

3.2. *Lee cyclogenesis*

Thirty cases of 'lee cyclogenesis' were identified in the study area from the AMPS surface pressure charts, with 29 cases having sufficient data available for input into composites. Twelve hourly composites of sea-level pressure, near-surface potential temperature and near-surface wind vectors for lee cyclogenesis cases are shown in Fig. 7. At −12 h (Fig. 7a), there is a lee trough between 140°E and 160°E along the East Antarctic coast. Over the coastal slopes, near-surface wind speeds of 20–30 m s^{-1} are directed offshore between these longitudes, associated with synoptically supported katabatic winds (Parish and Walker, 2006). Cyclogenesis occurs well south of the marginal sea ice zone. Over the next 12 h (Fig. 7b), the lee trough becomes amplified, and a closed circulation is attained at 0 h. After this (Fig. 7c), the composite cyclone moves northeastward into a weak low-level baroclinic zone. Figure 8 shows the composite 500 hPa geopotential heights and relative vorticity. Deep offshore flow exists over the continent, associated with a trough extending northwestward from the southern Ross Sea. Over the composite sequence in Fig. 8, this trough builds into Adélie Land and George V Land from Victoria Land (see Fig. 1 for locations) and amplifies. Cyclonic vorticity advection increases between −12 and 0 h just offshore of Adélie Land.

Under linear mountain wave theory, the formation of the lee trough in the composite sequence of Fig. 8 would result if the Rossby number,

$$\mathrm{Ro} = \frac{U}{|f|\,L}, \tag{4}$$

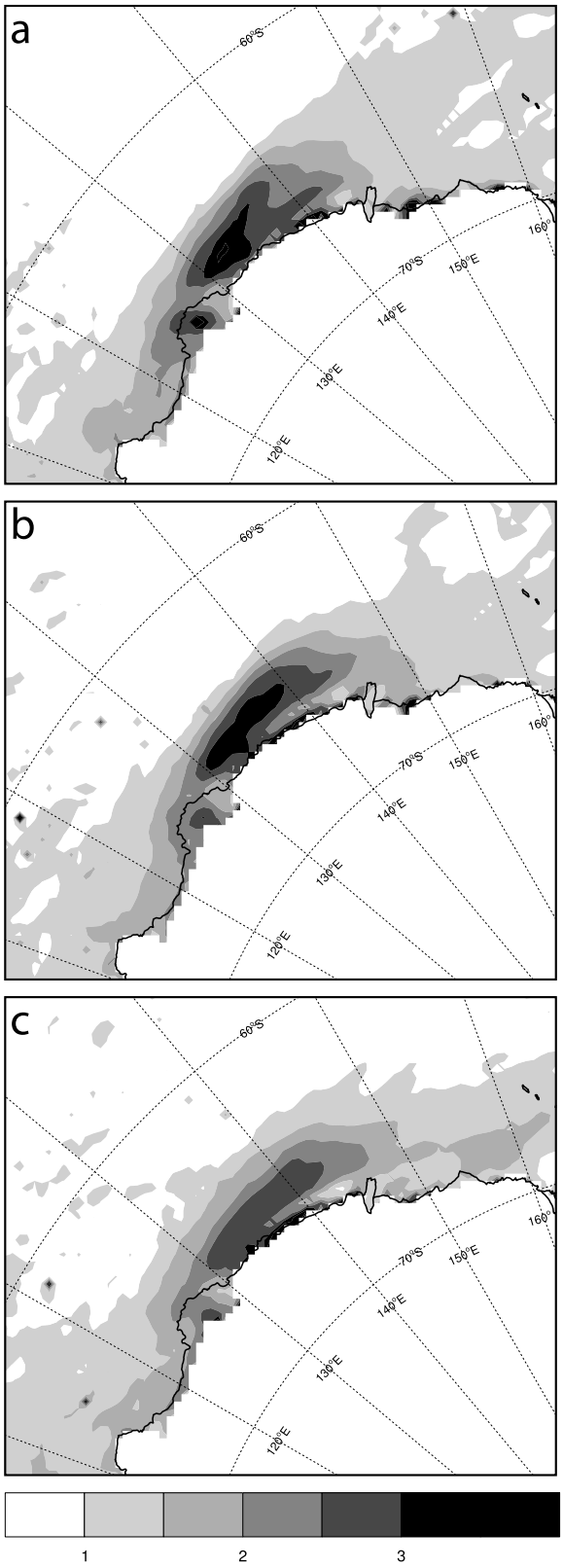

Fig. 5. Composite 900 hPa Eady growth rate (day^{-1}) at (a) −12 h, (b) −6 h and (c) 0 h.

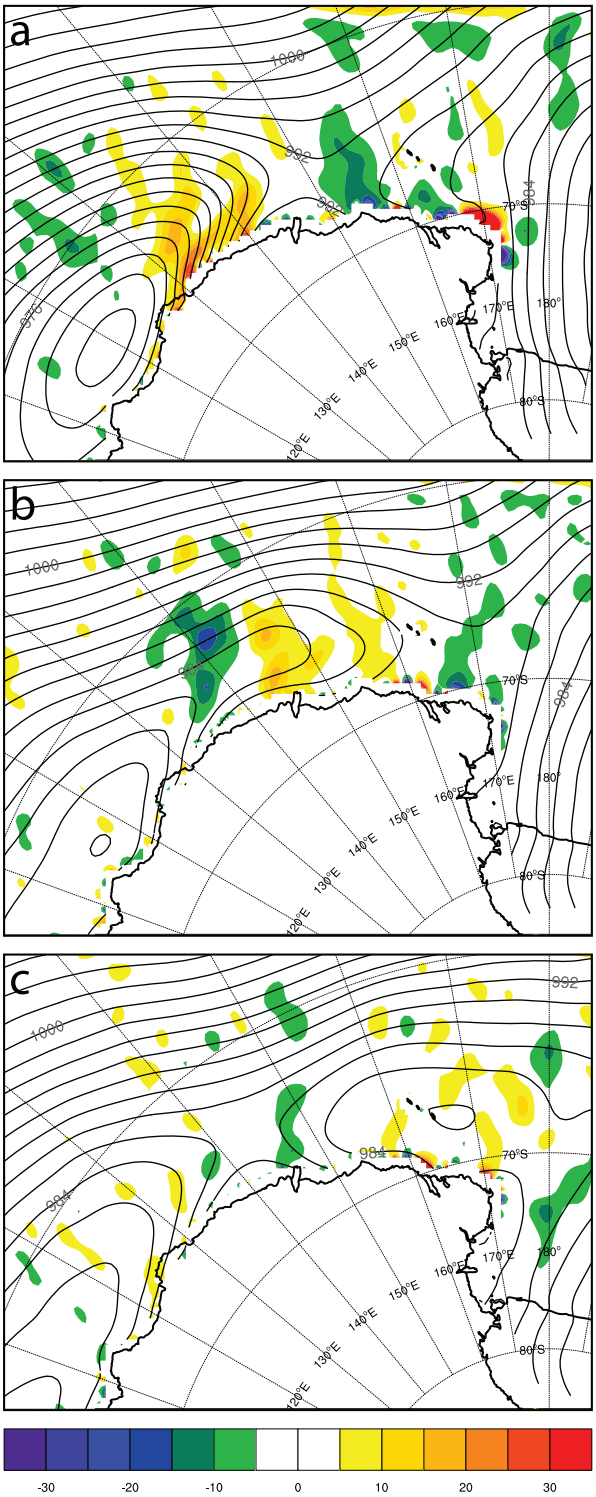

Fig. 6. 'Secondary Development' composites of 400–600 hPa layer $-2\nabla \cdot Q$, 10^{-16} K^{-1} s^{-3}, colour shaded, positive values imply upward vertical motion, negative values imply downward vertical motion) and sea-level pressure (hPa, black contours, contour interval 2 hPa) at (a) −12 h, (b) 0 h and (c) +12 h. Values masked over Ross Ice Shelf and western Ross Sea.

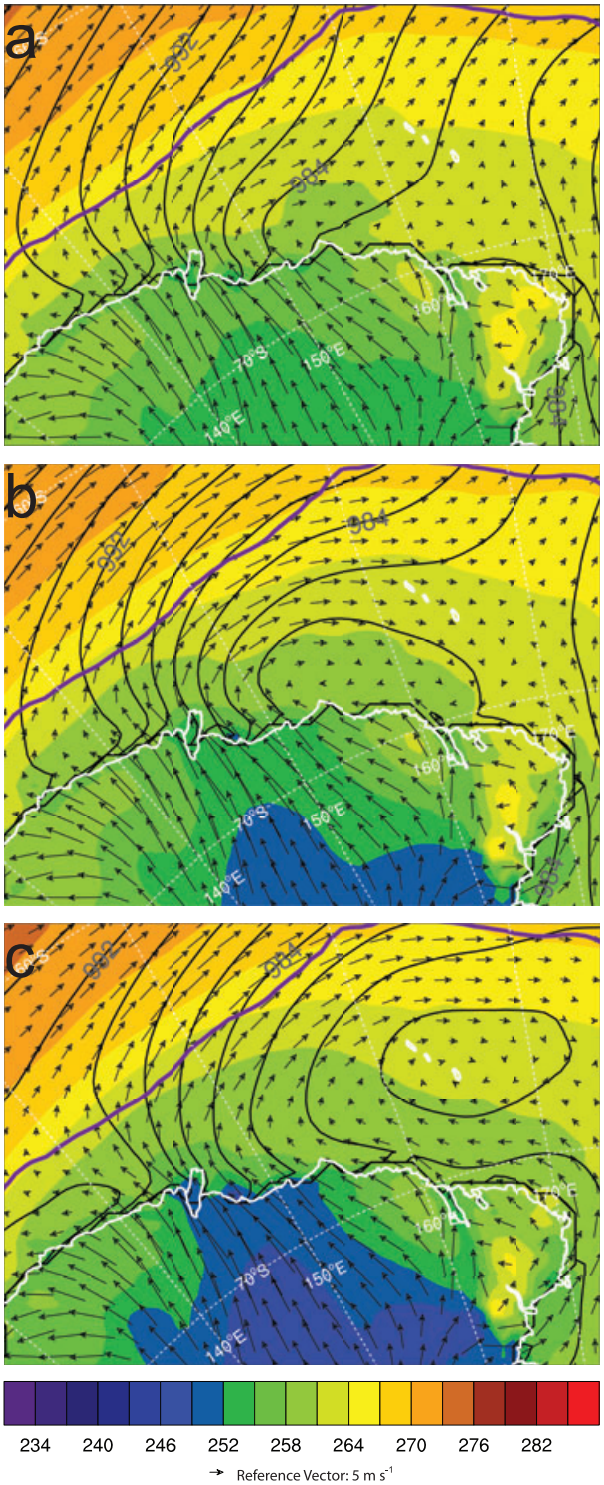

Fig. 7. 'Lee Cyclogenesis' composites of sea-level pressure (hPa, black contours, contour interval 2 hPa), potential temperature (K, colour shaded) at $\sigma = 0.9983$ (about 13 m AGL), and wind vectors (black arrows) at $\sigma = 0.9983$ at (a) −12 h, (b) 0 h and (c) +12 h. Composite 50% sea ice concentration isopleth delineated by purple line.

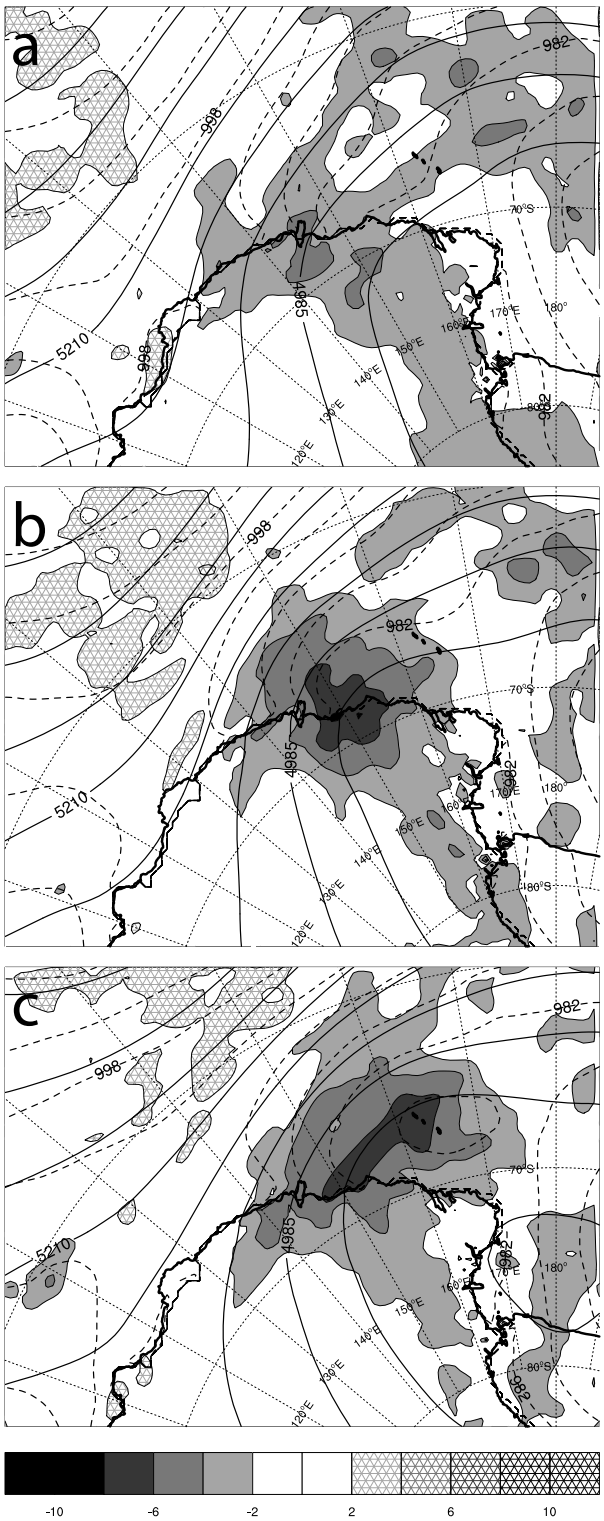

Fig. 8. 'Lee Cyclogenesis' composites of 500 hPa geopotential height (m, full contours), 500 hPa relative vorticity (10^{-5} s^{-1}, negative values solid shaded, positive values cross hatched) and sea-level pressure (hPa, dashed contours, contour interval 4 hPa) at (a) −12 h, (b) 0 h and (c) +12 h.

where U is a characteristic wind speed, L is the mountain half-width and f is the Coriolis parameter, is less than order unity (e.g. Peng et al., 1995). This situation is characteristic of flow in this region, with a large Coriolis parameter and wide mountain ridge. The result of such a flow regime is the generation of cyclonic vorticity in the lee. The generation of cyclonic vorticity can be described through the conservation of isentropic potential vorticity (PV) for adiabatic, frictionless flow,

$$-g\left(\zeta_\theta + f\right)\left(\frac{\partial \theta}{\partial p}\right), \tag{5}$$

where g is gravity, ζ_θ is isentropic relative vorticity and θ is potential temperature. Decreases in the magnitude of f (northward motion of the vortex) and the stability term (air in the column between two isentropes must remain there) dictate that ζ_θ must increase in magnitude. Surface pressure falls in the lee trough result from the adiabatic warming of the descending flow.

To explore the role of the potential temperature distribution on lee trough formation, Fig. 9 shows potential temperature and wind vectors at $\sigma = 0.8971$ (about 790 m AGL) at −6 h. This model level is above the boundary layer yet is still impacted by terrain effects. Pockets of cold air are located just offshore between 140°E and 150°E, compared to a relatively warm region offshore along transect E1–E2. Figure 10 shows cross sections of potential temperature, vertical velocity and horizontal velocity at −6 h along the transects shown in Fig. 9. Along transect W1–W2 (Fig. 10a), strong downward vertical motion is present along the coastal slopes, due to the intense katabatic winds in this region (Fig. 10b). The downward vertical motion sharply decreases near the coast, and a broad region of upward vertical motion offshore extends upwards to almost 2000 m ASL. Potential temperature decreases in this region, as the potentially cold near-surface air is transported upwards, in effect negating much of the adiabatic warming associated with broadscale descent off of Antarctica. The alternating phases of vertical motion offshore in Fig. 10a, along with inspection of individual cases, suggests a vertically propagating mountain wave regime. This region is also known for katabatic jumps (e.g. Pettré and André, 1991), which are similar to hydraulic jumps, and result in strong turbulence and upward vertical motion. Even though AMPS has insufficient horizontal spatial resolution to properly resolve katabatic jumps, which occur on spatial scales ∼100 m, it is certainly plausible that AMPS provides smoothed representations of them. Figure 11a shows potential temperature and wind vectors at $\sigma = 0.8129$ (about 1490 m AGL), and Fig. 11b shows horizontal velocity and potential temperature along transect W′1–W′2 in Fig. 11a for a lee cyclogenesis case. Figure 11b clearly illustrates the katabatic wind layer and katabatic jump at the base of the slope. While the structure of these features is beyond the scope of this paper, it is clear that large-amplitude mountain waves significantly modulate the offshore environment.

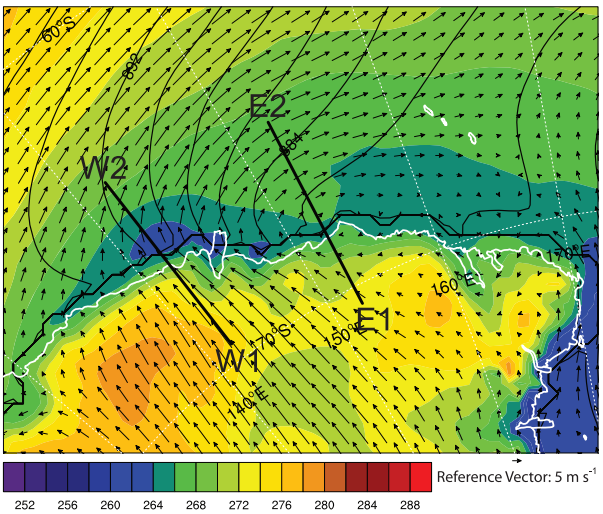

Fig. 9. 'Lee Cyclogenesis' composite of pressure (hPa, black contours, contour interval 2 hPa), potential temperature (K, colour shaded) and wind vectors (black arrows) at $\sigma = 0.8971$ (about 790 m AGL) at −6 h. Transects represent cross sections in Fig. 10.

The situation is different along transect E1–E2 (Fig. 10c), as here the coastal slopes are less steep than to the west, and katabatic winds are weaker (Fig. 10d). The vertical motions are damped compared to Fig. 10a, with only weak ascent offshore. These features are verified by the example of a lee cyclogenesis case in Fig. 11c, showing the weaker katabatic winds along transect E′1–E′2 in Fig. 11a. As a result of the downslope flow pattern near 152°E, this offshore region is favourable for lee trough formation due to the layer warming under 2.5 km height leading to surface pressure falls, compared to the region near 140°E, where adiabatic warming of the downslope flow is negated by the upward vertical motion. A lee trough becomes mobile and often undergoes cyclogenesis corresponding to arrival of upper level forcing, for example, a 500 hPa shortwave trough. This is apparent in the 500 hPa geopotential height composites shown in Figs 8a–c.

The offshore region near 152°E is also favourable for cyclogenesis since it involves the generation of low-level vorticity. The intense Adélie Land katabatic wind regime is isolated to the region between 140°E and 150°E, so that a region of shear vorticity is created to the east of the katabatic jet. Figure 12 shows vorticity on the $\sigma = 0.9791$ surface (about 155 m AGL) at 0 h. A region of enhanced cyclonic vorticity exists between 145°E and 155°E offshore, on the cyclonic-shear side of the katabatic jet.

In summary, the combination of enhanced low-level vorticity, adiabatic warming and associated lee trough development, and upper-level forcing results in a favourable region for cyclogenesis near 152°E. The Adélie Land katabatic wind regime is directly responsible for the enhanced low-level vorticity, while indirectly affecting lee trough development through large-amplitude mountain waves.

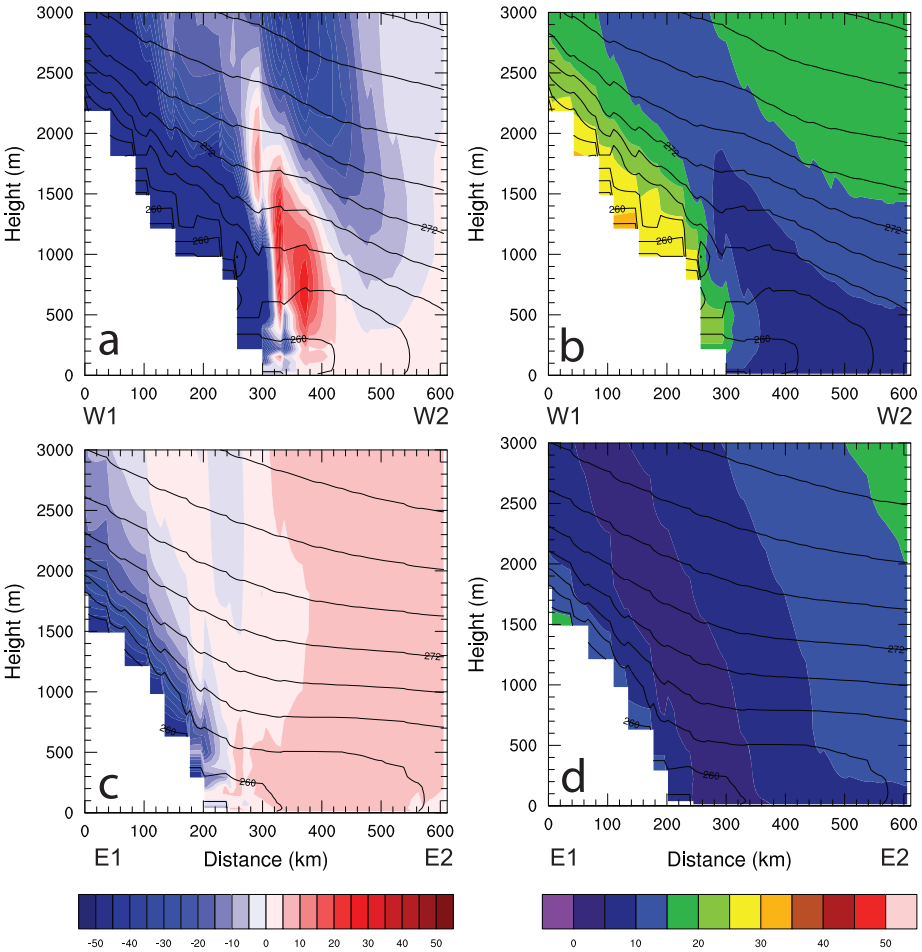

Fig. 10. 'Lee Cyclogenesis' composite cross sections at −6 h of (a) vertical velocity (mm s^{-1}, colour shaded) and potential temperature (K, black contours, contour interval 3 K) and (b) horizontal velocity (m s^{-1}, colour shaded) and potential temperature along western transect in Fig. 9. (c) and (d) same as (a) and (b) except along eastern transect in Fig. 9.

4. Cyclone tracking climatology

An analysis of cyclone tracking results from the MU tracking scheme (using AMPS output) is done to (i) place the 2003–2005 study period into a broader 'climatological context', (ii) track the cyclones that form in the study area, (iii) characterize the set of cyclones manually identified against an established data set and (iv) analyse the behaviour of the automated cyclone finding and tracking scheme in this region. AMPS cyclogenesis and cyclolysis density for 2003–2005 are plotted in Figs 13a and b, respectively. Cyclogenesis maxima can be seen to roughly correspond with the locations of secondary development (140°E–145°E) and east of 160°E for lee cyclogenesis. Cyclolysis is maximized in a belt between 60°S and 65°S. The prominent cyclolysis region found in several previous studies upstream near 120°E is also present here, with cyclolysis to the east near 150°E likely corresponding with newly developed cyclones that have a short lifetime. The density patterns in Fig. 13 broadly correspond with the mesoscale system density from Irving et al. (2010).

To gauge how the 2003–2005 time period compares to a longer record, standardized anomalies of cyclogenesis and cyclolysis from JRA-25 for the 2003–2005 period against the 1979–2007 period are shown in Fig. 14. The goal here is to gain a climatological perspective of the 2003–2005 period, and JRA-25 is appropriate for this task, as it goes back to 1979, compared to 2001 for AMPS. This analysis is restricted to synoptic-scale systems, as AMPS features more mesoscale systems than reanalysis products near the Antarctic coast (Uotila et al. 2009). For cyclogenesis in the study area (60°S-coast, 140°E–160°E), positive anomalies are found along 140°E and negative anomalies near the coast at 150°E, all of which are less than 1 standard deviation in magnitude. Greater cyclogenesis is found north of the study area (north of 60°S). Cyclolysis anomalies are positive upstream (near 120°E), but negative in the study area. Anomalies were also plotted for each year individually, and for each individual season (not shown). Only isolated areas within and near the study region exceed 2 standard deviations. Therefore,

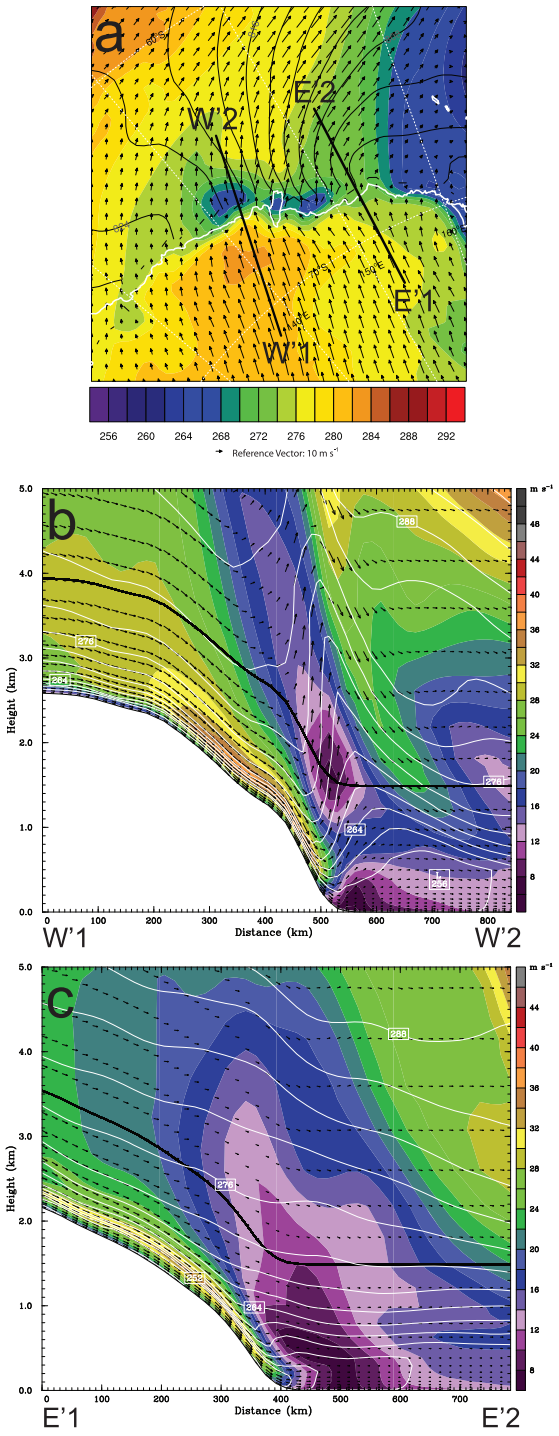

Fig. 11. (a) Pressure (hPa, black contours, contour interval 2 hPa), potential temperature (K, colour shaded) and wind vectors (black arrows) at $\sigma = 0.8129$ (about 1490 m AGL) at 0600 UTC 14 May 2004 (6 h before cyclogenesis). (b) and (c) Cross sections of potential temperature (K, white contours, contour interval 3 K), horizontal velocity (m s^{-1}, colour shaded), and circulation vectors along transects W′1–W′2 and E′1–E′2 in (a), respectively, at 0600 UTC 14 May 2004. Thick black lines represent level of $\sigma = 0.8129$.

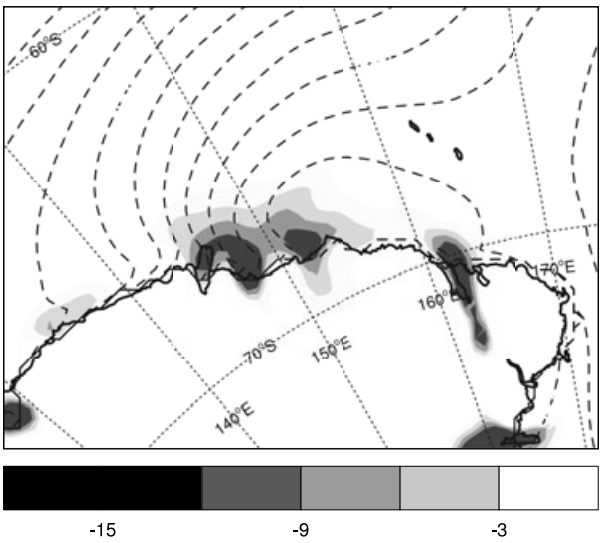

Fig. 12. 'Lee Cyclogenesis' composite of relative vorticity (10^{-5} s^{-1}, negative values only, shaded) at $\sigma = 0.9791$ (about 155 m AGL) and sea-level pressure (hPa, dashed contours, contour interval 2 hPa) at 0 h.

the 2003–2005 period is found to be representative of the overall climatology of the region.

A direct comparison between cyclogenesis cases found in the automated scheme and those identified manually is now discussed. Within the study area, 202 cyclogenesis cases are identified in the automated scheme, compared to 132 cases identified manually. This ratio is consistent with that of Keable et al. (2002), who compare 500 hPa cyclones from the MU tracking scheme with those identified manually using National Centers for Environmental Prediction–National Center for Atmospheric Research (NCEP–NCAR) reanalysis data for January 1996. There, 129 cyclones were identified in the automated scheme, compared to 65 cyclones identified manually.

In this analysis, the manually identified cyclogenesis cases were fairly evenly distributed between years, with 47 in 2003, 41 in 2004 and 44 in 2005. Seasonally, the greatest totals are in autumn (MAM), winter (JJA) and spring (SON), with 38, 39 and 34 cyclones, respectively. Only 21 cases were identified in summer (DJF). 127 (of 132 possible) direct matches were found between the manual and automated tracking. The tracks of these cyclones in the automated scheme are shown in Fig. 15a. Cyclones generally track eastward through the study area and out towards the Ross Sea, with the longer-lived cyclones spiraling into the Marie Byrd Land coast. These tracks are similar to the rubber band track density contours shown in Hoskins and Hodges (2005, their Fig. 6a). Figure 15a also shows that, according to the MU tracking scheme, many of the matched cyclones form outside of the study area, primarily to the west but also to the north and east.

Tracks from the 53 'secondary development' cases are isolated in Fig. 15b. Of the 53 cyclones, 22 form in the study

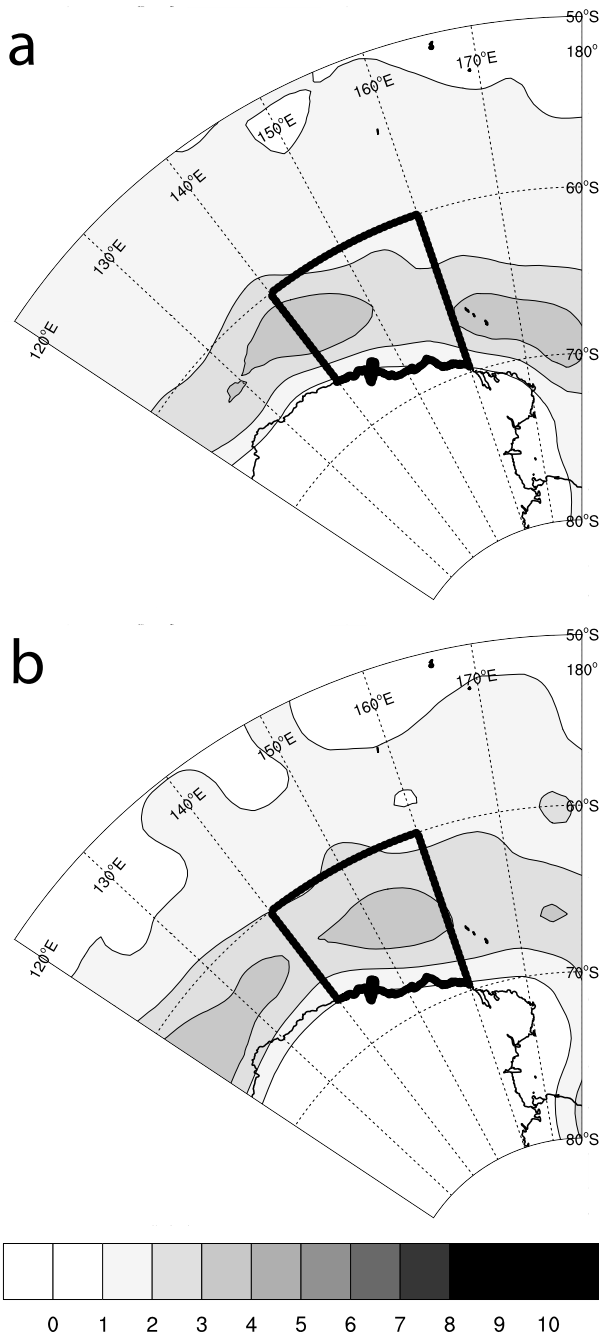

Fig. 13. (a) Cyclogenesis density and (b) cyclolysis density for 2003–2005 period using AMPS output in MU tracking scheme. Units are 10^{-3} cyclones ($^\circ$ lat)$^{-2}$ day^{-1}. AMPS data is at 0.5° by 0.5° resolution. Bold outline represents manual cyclone tracking study area (140°E–160°E, 60°S-coast).

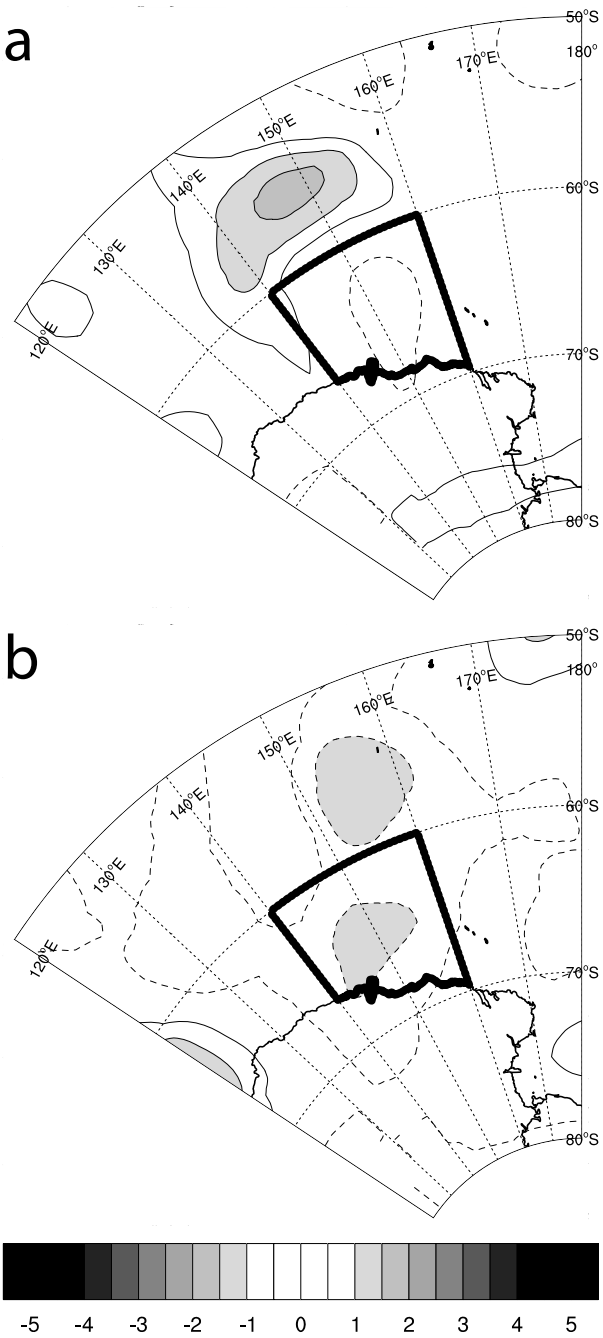

Fig. 14. JRA-25 standardized anomalies of (a) cyclogenesis density and (b) cyclolysis density of 2003–2005 period against 1979–2007 period. Contour interval 0.5 standard deviations (solid line positive, dashed line negative), magnitudes greater than 1 standard deviation shaded. Bold outline represents manual cyclone tracking study area (140°E–160°E, 60°S-coast).

area, 27 form to the west of 140°E, 3 form to the northwest and 1 is not accounted. Forty of the 52 identified cyclones form as 'open' cyclones, meaning they have no closed isobars. The large number of open cyclones and those forming to the west of 140°E implies that manually identified cyclones are more mature and well-developed compared to the automated cases. Based on manual inspection of the 27 systems that form to the west, and the composite sequence in Fig. 2, the automated scheme is

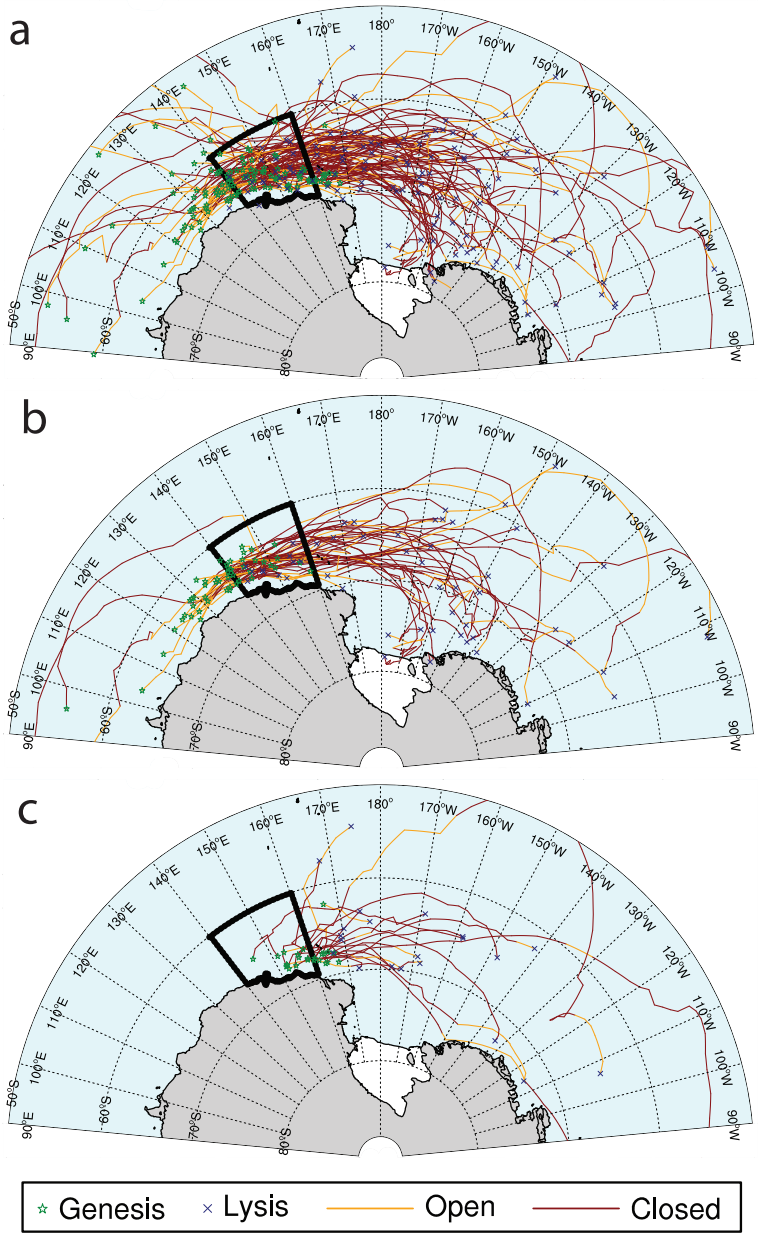

Fig. 15. Cyclone tracks from MU tracking scheme for (a) cyclones matched between automated tracking and manual identification, (b) matched 'secondary development' and (c) matched 'lee cyclogenesis'. Stars denote genesis points, crosses denote lysis points, red lines represent closed cyclones, yellow lines represent open cyclones. Bold outline represents manual cyclone tracking study area (140°E–160°E, 60°S-coast).

misidentifying modulation of the isobars early in the secondary development process (Fig. 2a,b) as cyclogenesis. The mesoscale system density maximum west of 140°E in Irving et al. (2010) may be a reflection of this. For the 30 'lee cyclogenesis' cases, the tracks are shown in Fig. 15c. 14 cyclones form in the study area, 11 form to the east, 1 merges with another cyclone and 4 are not accounted for. Only 13 cyclones are 'open' at initiation. Generally, these cyclones have a weaker signature in the pressure field compared to 'secondary development' cyclones. As a result, the automated scheme identifies these cyclones after the manual scheme, and often east of 160°E.

Of the 202 cyclogenesis cases identified in the study area by the automated scheme, 146 are not directly matched with cases from the manual analysis. Of the 146 cases, 40 are similar to the patterns seen early in 'secondary development' (Fig. 2a,b). Composite sea-level pressure and near-surface winds for these 40 cases are shown in Fig. 16. Unlike the composites for the manually identified cyclones in Fig. 2, a new cyclone does not form east of the existing cyclone. Instead, a trough extends eastward with time, while the existing cyclone propagates farther east and remains stronger than the corresponding cyclone in Fig. 2. The evolution of the feature appears to be dependent upon

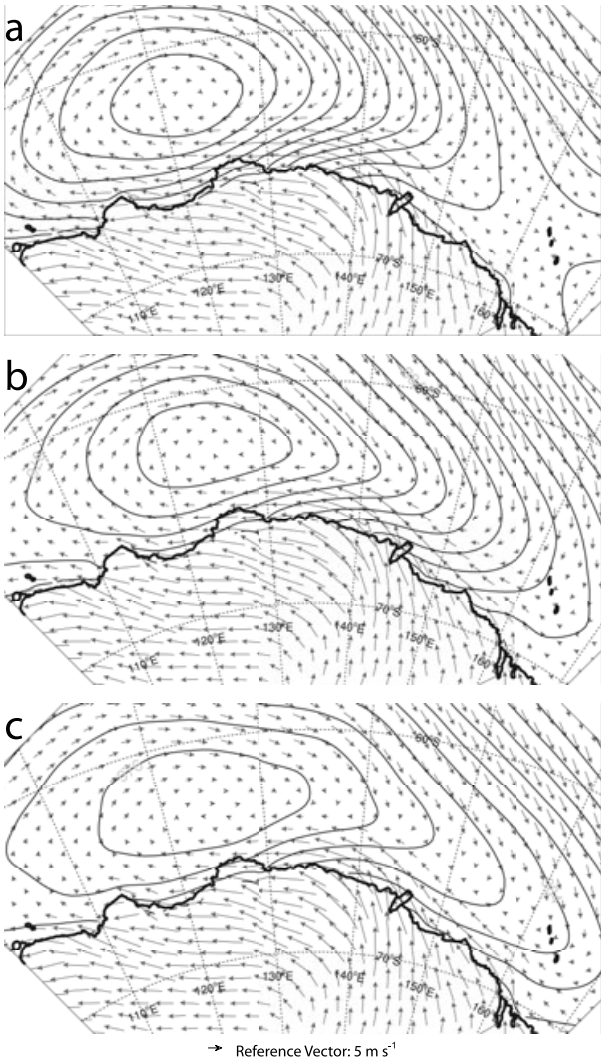

Fig. 16. 'Weak Secondary Development' (40 cyclones identified by MU tracking scheme but not manually) composites of sea-level pressure (hPa, black contours, contour interval 2 hPa) and wind vectors (black arrows) at $\sigma = 0.9983$ at (a) −12 h, (b) 0 h and (c) +12 h. Note that map projection is rotated 45° clockwise from Fig. 1 for clarity.

the position and intensity of the existing cyclone to the west. A stronger existing cyclone that propagates farther east maintains a strong easterly jet and prevents a new cyclone from forming. Classification of these cases as cyclones is questionable, given that they are shallow, terrain-induced features. As a result, the automated scheme may be overestimating coastal cyclogenesis near Adélie Land and elsewhere around Antarctica.

5. Conclusions

Physical mechanisms responsible for cyclogenesis in the Adélie Land coastal region are explored in this study. Composite analysis of the 2003–2005 period is done for the two primary cyclogenesis patterns. 'Secondary development' cyclones form near 145°E along the warm front of an existing dissipating cyclone to the west near 120°E. Barrier winds and katabatic winds increase baroclinicity and cyclonic vorticity at low-levels, providing a favourable environment for cyclogenesis. 'Lee cyclogenesis' cyclones form near 152°E, associated with deep offshore southerly flow leading to formation of a lee trough. The position of the lee trough and subsequent cyclogenesis is favoured near 152°E due to a warm potential temperature anomaly in low-levels, compared to farther west near 140°E, where any effects of adiabatic warming are negated by large-amplitude mountain waves. Low-level cyclonic vorticity is generated on the cyclonic-shear side of the Adélie Land katabatic jet.

Comparison of manually identified cyclones with those from the MU tracking scheme shows general agreement, with cyclones forming near Adélie Land being part of the Southern Ocean cyclone track. For 'secondary development' cases, cyclones develop upstream in the automated scheme compared to the manual identification. This, combined with instances of weak 'secondary development', where a cyclone is identified in the automated scheme but not manually, shows that the automated scheme is often identifying shallow features that result solely from near-surface pressure gradient modulation due to barrier/katabatic winds. Tracking schemes based on vorticity, like that of Hoskins and Hodges (2005), may be subject to this issue as well, as cyclonic vorticity maxima can extend upwards to 850 hPa.

This study shows that katabatic winds do have a role in cyclogenesis. For 'secondary development', katabatic winds contribute to the generation of low-level cyclonic vorticity and baroclinicity along the coast. For 'lee cyclogenesis', katabatic winds indirectly affect cyclogenesis through differences in low-level temperatures offshore, and more directly through cyclonic vorticity generation on the cyclonic-shear side of the jet. The implication of Hoskins and Hodges (2005) that katabatic winds only have a role in mesoscale cyclone development is not supported here. Parish and Bromwich (1998) suggested a connection between katabatic wind 'confluence zones', like the one in Adélie Land, and synoptic-scale cyclone activity. The Adélie Land katabatic winds are also an important factor in the generation of the polar front jet just offshore (Kidston et al., 2009), which likely steers cyclones to the east towards the Ross Sea. Cyclogenesis is found to be dependent upon the proper juxtaposition of an existing dissipating cyclone to the west (for 'secondary development'), the Adélie Land katabatic wind regime, and favourable upper tropospheric circulation. Based upon the locations of strong coastal winds (Parish and Bromwich, 2007) and high cyclolysis frequency (Simmonds et al., 2003; Hoskins and Hodges, 2005), Antarctic coastal cyclogenesis would be expected to be most frequent near Adélie Land.

6. Acknowledgments

This work was supported by NASA via Grant NNG04GM26G and the National Science Foundation Office of Polar Programs via UCAR Subcontract S01-22901. Parts of this work were made possible by a grant from the Australian Research Council. Petteri Uotila provided UM tracking scheme output from AMPS. Byrd Polar Research Center Contribution Number 1408.

References

Barker, D. M., Huang, W., Guo, Y.-R., Bourgeois, A. J. and Xiao, Q. N. 2004. A three dimensional variational data assimilation system for MM5: implementation and initial results. *Mon. Wea. Rev.* **132**, 897–914.

Berbery, E. H. and Vera, C. S. 1996. Characteristics of the Southern Hemisphere winter storm track with filtered and unfiltered data. *J. Atmos. Sci.* **53**, 468–481.

Bromwich, D. H. 1989. Subsynoptic-scale cyclonic developments in the Ross Sea sector of the Antarctic. In: *Polar and Arctic Lows*, (eds P. F. Twitchell, E. A. Rasmussen, K. L. Davidson). A. Deepak Publishers, Hampton, VA, USA, 331–345.

Bromwich, D. H. 1991. Mesoscale cyclogenesis over the southwestern Ross Sea linked to strong katabatic winds. *Mon. Wea. Rev.* **119**, 1736–1752.

Bromwich, D. H., Cassano, J. J., Klein, T., Heinemann, G., Hines, K. M. and co-authors. 2001. Mesoscale modeling of katabatic winds over Greenland with the Polar MM5. *Mon. Wea. Rev.* **129**, 2290–2309.

Bromwich, D. H., Fogt, R. L., Hodges, K. E. and Walsh, J. E. 2007. A tropospheric assessment of the ERA-40, NCEP, and JRA-25 global reanalyses in the polar regions. *J. Geophys. Res.* **112**, doi:10.1029/2006JD007859.

Bromwich, D. H., Monaghan, A. J., Manning, K. W. and Powers, J. G. 2005. Real-time forecasting for the Antarctic: an evaluation of the Antarctic Mesoscale Prediction System (AMPS). *Mon. Wea. Rev.* **133**, 579–603.

Bromwich, D. H., Monaghan, A. J., Powers, J. G., Cassano, J. J., Wei, H.-L. and co-authors. 2003. Antarctic mesoscale prediction system (AMPS): a case study from the 2000–01 field season. *Mon. Wea. Rev.* **131**, 412–433.

Carleton, A. M. 1979. A synoptic climatology of satellite-observed extratropical cyclone activity for the Southern Hemisphere winter. *Arch. Meteorol. Geophys. Bioklimatol.* **B27**, 265–279.

Carleton, A. M. 1983. Variations in Antarctic sea ice conditions and relationships with Southern Hemisphere cyclonic activity, winters 1973–77. *Arch. Met. Geoph. Biocl., Ser. B* **32**, 1–22.

Carleton, A. M. 1992. Synoptic interactions between Antarctica and lower latitudes. *Aust. Meteorol. Mag.* **40**, 129–147.

Carleton, A. M. and Carpenter, D. A. 1990. Satellite climatology of "polar lows" and broadscale climatic associations for the Southern Hemisphere. *Int. J. Climatol.* **10**, 219–246.

Carleton, A. M. and Fitch, M. 1993. Synoptic aspects of Antarctic mesocyclones. *J. Geophys. Res.* **98**, 12 997–13 018.

Carleton, A. M. and Song, Y. 1997. Synoptic climatology, and intrahemispheric associations, of cold air mesocyclones in the Australasian sector. *J. Geophys. Res.* **102**, 13 873–13 888.

Carlson, T. N. 1991. *Mid-Latitude Weather Systems*. American Meteorological Society, Boston, 507 pp.

Carrasco, J. F. 1994. *Dynamics of Mesoscale Cyclogenesis Adjacent to The Pacific Coast of Antarctica*. Ph.D. dissertation, Atmospheric Sciences Program, The Ohio State University, 286 pp.

Carrasco, J. F. and Bromwich, D. H. 1993. Mesoscale cyclogenesis dynamics over the southwestern Ross Sea, Antarctica. *J. Geophys. Res.* **98**, 12 973–12 995.

Carrasco, J. F. and Bromwich, D. H. 1995. A case of a midtropospheric subsynoptic-scale vortex development over the Ross Sea and Ross Ice Shelf area, Antarctica. *Antarct. Sci.* **7**, 199–210.

Carrasco, J. F., Bromwich, D. H. and Liu, Z. 1997a. Mesoscale cyclone activity over Antarctica during 1991, Part 1: Marie Byrd Land. *J. Geophys. Res.* **102**, 13 923–13 937.

Carrasco, J. F., Bromwich, D. H. and Liu, Z. 1997b. Mesoscale cyclone activity over Antarctica during 1991, Part 2: Near the Antarctic Peninsula. *J. Geophys. Res.* **102**, 13 939–13 954.

Carrasco, J. F., Bromwich, D. H. and Monaghan, A. J. 2003. Distribution and characteristics of mesoscale cyclones in the Antarctic: Ross Sea eastward to the Weddell Sea. *Mon. Wea. Rev.* **131**, 289–301.

Cassano, J. J., Box, J. E., Bromwich, D. H., Li, L. and Steffen, K. 2001. Evaluation of Polar MM5 simulations of Greenland's atmospheric circulation. *J. Geophys. Res.* **106**, 33 867–33 889.

Eady, E. T. 1949. Long waves and cyclone waves. *Tellus* **1**, 33–52.

Engels, R. and Heinemann, G. 1996. Three-dimensional structures of summertime Antarctic meso-scale cyclones: Part II: Numerical simulations with a limited area model. *Atmos.-Ocean Syst.* **4**, 181–208.

Fantini, M. and Buzzi, A. 1993. Numerical experiments on the possible mechanism of cyclogenesis in the Antarctic region. *Tellus* **45A**, 99–113.

Fogt, R. L. and Bromwich, D. H. 2008. Atmospheric moisture and cloud cover characteristics forecast by AMPS. *Wea. Forecast.* **23**, 914–930.

Gallée, H. 1995. Simulation of mesocyclonic activity in the Ross Sea, Antarctica. *Mon. Wea. Rev.* **123**, 2051–2069.

Gallée, H. 1996. Mesoscale atmospheric circulation over the southwestern Ross Sea sector, Antarctica. *J. Appl. Meteorol.* **35**, 1129–1141.

Godfred-Spenning, C. R. and Simmonds, I. 1996. An analysis of Antarctic sea-ice and extratropical cyclone associations. *Int. J. Climatol.* **16**, 1315–1332.

Grell, G. A., Dudhia, J. and Stauffer, D. R. 1995. A description of the Fifth-Generation Penn State/NCAR Mesoscale Model (MM5). NCAR Tech. Note TN-398+STR, 122 pp.

Guo, Z., Bromwich, D. H. and Cassano, J. J. 2003. Evaluation of Polar MM5 simulations of Antarctic atmospheric circulation. *Mon. Wea. Rev.* **131**, 384–411.

Heinemann, G. and Klein, T. 2003. Simulations of topographically forced mesocyclones in the Weddell Sea and the Ross Sea region of Antarctica. *Mon. Wea. Rev.* **131**, 302–316.

Hodges, K. I. 1995. Feature tracking on the unit sphere. *Mon. Wea. Rev.* **123**, 3458–3465.

Hodges, K. I. 1996. Spherical nonparametric estimators applied to UGAMP model integration for AMIP. *Mon. Wea. Rev.* **124**, 2914–2932.

Hodges, K. I. 1999. Adaptive constraints for feature tracking. *Mon. Wea. Rev.* **127**, 1362–1373.

Holton, J. R. 1992. *An Introduction to Dynamic Meteorology*. Academic Press, San Diego, 511 pp.

Hoskins, B. J., Draghici, I. and Davies, H. C. 1978. A new look at the ω-equation. *Q. J. R. Meteorol Soc.* **104**, 31–38.

Hoskins, B. J. and Hodges, K. I. 2005. A new perspective on Southern Hemisphere storm tracks. *J. Clim.* **18**, 4108–4129.

Hudson, D. A. and Hewitson, B. C. 2001. The atmospheric response to a reduction in summer Antarctic sea-ice extent. *Clim. Res.* **16**, 79–99.

Irving, D., Simmonds, I. and Keay, K. 2010. Mesoscale cyclone activity over the ice-free Southern Ocean: 1999–2008. *J. Clim.* **23**, 5404–5420.

Jones, D. A. and Simmonds, I. 1993. A climatology of Southern Hemisphere extratropical cyclones. *Clim. Dyn.* **9**, 131–145.

Keable, M., Simmonds, I. and Keay, K. 2002. Distribution and temporal variability of 500 hPa cyclone characteristics in the Southern Hemisphere. *Int. J. Climatol.* **22**, 131–150.

Keller, L. M., Weidner, G. A., Stearns, C. R., Whittaker, M. T. and Holmes, R. E. 1997. Antarctic Automatic Weather Station Data for the Calendar Year 1995. Department of Atmospheric and Oceanic Sciences, University of Wisconsin-Madison, 33 pp. (Available from the Department of Atmospheric and Oceanic Sciences, University of Wisconsin-Madison, Madison, WI 53706).

Kidston, J., Renwick, J. A. and McGregor, J. 2009. Hemispheric-scale seasonality of the Southern Annular Mode and impacts on the climate of New Zealand. *J. Clim.* **22**, 4759–4770.

Klein, T. and Heinemann, G. 2001. On the forcing mechanisms of mesocyclones in the eastern Weddell Sea region, Antarctica: process studies using a mesoscale numerical model. *Meteorol. Z.* **10**, 113–122.

Lambert, S. J. 1988. A cyclone climatology of the Canadian Climate Centre general circulation model. *J. Clim.* **1**, 109–115.

Le Marshall, J. F. and Kelly, G. A. M. 1981. A January and July climatology of the Southern Hemisphere based on daily numerical analyses 1973–77. *Aust. Meteorol. Mag.* **29**, 115–123.

Le Treut, H. and Kalnay, E. 1990. Comparison of observed and simulated cyclone frequency distribution as determined by an objective method. *Atmosfera* **3**, 57–71.

Lim, E.-P. and Simmonds, I. 2007. Southern Hemisphere winter extratropical cyclone characteristics and vertical organization observed with the ERA-40 data in 1979–2001. *J. Clim.* **20**, 2675–2690.

Madigan, C. T. 1929. Tabulated and reduced records of the Cape Denison station, Adélie Land, Austr. Antarct. Expedition 1911–1914. *Sci. Rep. Ser. B*, Vol. 4. Government Printer (Sydney), 286 pp.

Mawson, D. 1915. *The Home of the Blizzard*. Volume 1, 349 pp, Volume 2, 338 pp, William Heinemann Co., London.

Menendez, C. G., Serafini, V. and Le Treut, H. 1999. The effect of sea-ice on the transient atmospheric eddies of the Southern Hemisphere. *Clim. Dyn.* **15**, 659–671.

Monaghan, A. J., Bromwich, D. H., Powers, J. G. and Manning, K. W. 2005. The climate of the McMurdo, Antarctica, region as represented by one year of forecasts from the Antarctic Mesoscale Prediction System. *J. Clim.* **18**, 1174–1189.

Murphy, B. F. and Simmonds, I. 1993. An analysis of strong wind events simulated in a GCM near Casey in the Antarctic. *Mon. Wea. Rev.* **121**, 522–534.

Murray, R. J. and Simmonds, I. 1991. A numerical scheme for tracking cyclone centres from digital data. Part I: Development and operation of the scheme. *Aust. Meteorol. Mag.* **39**, 155–166.

Nakamura, H. and Shimpo, A. 2004. Seasonal variations in the Southern Hemisphere storm tracks and jet streams as revealed in a reanalysis dataset. *J. Clim.* **17**, 1828–1844.

Nuss, W. A. and Titley, D. W. 1994. Use of multiquadric interpolation for meteorological objective analysis. *Mon. Wea. Rev.* **122**, 1611–1631.

Onogi, K., Tsutsui, J., Koide, H., Sakamoto, M., Kobayashi, S. and co-authors. 2007. The JRA-25 Reanalysis. *J. Meteorol. Soc. Japan* **85**, 369–432.

Parish, T. R. and Bromwich, D. H. 1998. A case study of Antarctic katabatic wind interaction with large-scale forcing. *Mon. Wea. Rev.* **126**, 199–209.

Parish, T. R. and Bromwich, D. H. 2007. Reexamination of the near-surface airflow over the Antarctic continent and implications on atmospheric circulations at high southern latitudes. *Mon. Wea. Rev.* **135**, 1961–1973.

Parish, T. R. and Walker, R. 2006. A re-examination of the winds of Adélie Land, Antarctica. *Aust. Meteorol. Mag.* **55**, 105–117.

Patoux, J., Foster, R. C. and Brown, R. A. 2003. Global pressure fields from scatterometer winds. *J. Appl. Meteorol.* **42**, 813–826.

Patoux, J., Yuan, X. and Li, C. 2009. Satellite-based midlatitude cyclone statistics over the Southern Ocean: 1. Scatterometer-derived pressure fields and storm tracking. *J. Geophys. Res.* **114**, doi:10.1029/2008JD010873.

Peng, M. S., Li, S.-W., Chang, S. W. and Williams, R. T. 1995. Flow over mountains: Coriolis force, transient troughs and three dimensionality. *Q. J. R. Meteorol. Soc.* **121**, 593–613.

Pettré, P. and André, J. C. 1991. Surface-pressure change through Loewe's Phenomenon and katabatic flow jumps: Study of two cases in Adélie Land, Antarctica. *J. Atmos. Sci.* **48**, 557–571.

Powers, J. G., Monaghan, A. J., Cayette, A. M., Bromwich, D. H., Kuo, Y.-H. and co-authors. 2003. Real-time mesoscale modeling over Antarctica. *Bull. Am. Meteorol. Soc.* **84**, 1533–1545.

Schlosser, E., Duda, M. G., Powers, J. G. and Manning, K. W. 2008. Precipitation regime of Dronning Maud Land, Antarctica, derived from Antarctic Mesoscale Prediction System (AMPS) archive data. *J. Geophys. Res.* **113**, doi:10.1029/2008JD009968.

Schwerdtfeger, W. 1984. *Weather and Climate of the Antarctic*. Elsevier, Amsterdam, 261 pp.

Simmonds, I. and Budd, W. F. 1991. Sensitivity of the Southern Hemisphere circulation to leads in the Antarctic pack ice. *Q. J. R. Meteorol. Soc.* **117**, 1003–1024.

Simmonds, I., Keay, K. and Lim, E.-P. 2003. Synoptic activity in the seas around Antarctica. *Mon. Wea. Rev.* **131**, 272–288.

Simmonds, I. and Lim, E.-P. 2009. Biases in the calculation of Southern Hemispheric mean baroclinic eddy growth rate. *Geophys. Res. Lett.* **36**, doi:10.1029/2008GL036320.

Simmonds, I. and Murray, R. J. 1999. Southern extratropical cyclone behavior in ECMWF analyses during the FROST special observing periods. *Wea. Forecast.* **14**, 878–891.

Simmonds, I., Murray, R. J. and Leighton, R. M. 1999. A refinement of cyclone tracking methods with data from FROST. *Aust. Meteorol. Mag.* Special Issue, 35–49.

Simmonds, I. and Wu, X. 1993. Cyclone behaviour response to changes in winter Southern Hemisphere sea-ice concentration. *Q. J. R. Meteorol. Soc.* **119**, 1121–1148.

Sinclair, M. R. 1994. An objective cyclone climatology for the Southern Hemisphere. *Mon. Wea. Rev.* **122**, 2239–2256.

Sinclair, M. R. 1995. A climatology of cyclogenesis for the Southern Hemisphere. *Mon. Wea. Rev.* **123**, 1601–1619.

Sinclair, M. R. 1997. Objective identification of cyclones and their circulation, intensity, and climatology. *Wea. Forecast.* **12**, 595–612.

Steinhoff, D. F., Bromwich, D. H., Lambertson, M., Knuth, S. L. and Lazzara, M. A. 2008. A dynamical investigation of the May 2004 McMurdo Antarctica severe wind event using AMPS. *Mon. Wea. Rev.* **136**, 7–26.

Streten, N. A. 1968. Some aspects of high latitude Southern Hemisphere summer circulation as viewed by ESSA 3. *J. Appl. Meteorol.* **7**, 324–332.

Streten, N. A. and Troup, A. J. 1973. A synoptic climatology of satellite observed cloud vortices over the Southern Hemisphere. *Q. J. R. Meteorol. Soc.* **99**, 56–72.

Taljaard, J. J. 1967. Development, distribution, and movement of cyclones and anticyclones in the Southern Hemisphere during IGY. *J. Appl. Meteorol.* **6**, 973–987.

Trenberth, K. E. and Fasullo, J. T. 2010. Simulation of present-day and twenty-first-century energy budgets of the Southern Oceans. *J. Clim.* **23**, 440–454.

Turner, J., Lachlan-Cope, T. A., Warren, D. E. and Duncan, C. N. 1993. A mesoscale vortex over Halley Station, Antarctica. *Mon. Wea. Rev.* **121**, 1317–1336.

Turner, J., Marshall, G.J. and Lachlan-Cope, T. A. 1998. Analysis of synoptic-scale low pressure systems within the Antarctic Peninsula sector of the circumpolar trough. *Int. J. Climatol.* **18**, 253–280.

Uotila, P., Pezza, A. B., Cassano, J. J., Keay, K. and Lynch, A. H. 2009. A comparison of low pressure statistics derived from a high resolution NWP output and three re-analysis products over the Southern Ocean. *J. Geophys. Res.* **114**, doi:10.1029/2008JD011583.

Uotila, P., Vihma, T., Pezza, A. B., Simmonds, I., Keay, K. and Lynch, A. H. 2011. Relationships between Antarctic cyclones and surface conditions as derived from high resolution NWP data. *J. Geophys. Res.* **116**, doi:10.1029/2010JD015358.

Walsh, K. J. E., Simmonds, I. and Collier, M. 2000. Sigma-coordinate calculation of topographically forced baroclinicity around Antarctica. *Dyn. Atmos. Oceans* **33**, 1–29.

Watkins, A. B. and Simmonds, I. 1995. Sensitivity of numerical prognoses to Antarctic sea ice distribution. *J. Geophys. Res.* **100**, 22 681–22 696.

Wernli, H. and Schwierz, C. 2006. Surface cyclones in the ERA-40 dataset (1958–2001). Part 1: Novel identification method and global climatology. *J. Atmos. Sci.* **63**, 2486–2507.

Yuan, X., Patoux, J. and Li, C. 2009. Satellite-based midlatitude cyclone statistics over the Southern Ocean: 2. Tracks and surface fluxes. *J. Geophys. Res.* **114**, doi:10.1029/2008JD010874.